Human primary motor cortex represents evidence for a perceptual decision before motor response

Sebastian Bitzer*[1], Hame Park*[2, 3], Burkhard Maess[4], Katharina von Kriegstein[1,4], Stefan J. Kiebel[1]

* joint first authorship
[1] Department of Psychology, Technische Universität Dresden, Germany
[2] Department for Cognitive Neuroscience, Faculty of Biology, Bielefeld University, Bielefeld, Germany
[3] Cognitive Interaction Technology – Center of Excellence, Bielefeld University, Bielefeld, Germany
[4] Max Planck Institute for Human Cognitive and Brain Sciences, Leipzig, Germany

Corresponding author: Sebastian Bitzer, Department of Psychology, Technische Universität Dresden, 01062 Dresden, Germany, E-mail: sebastian.bitzer@tu-dresden.de.

Keywords: perceptual decision making, MEG, human, primary motor cortex, posterior cingulate cortex, within-trial analysis, decision evidence

Abstract

Perceptual decision making involves a complex network of brain regions including premotor and motor cortices. Premotor areas activate in proportion to the available evidence, thus anticipating the movements required to indicate the still developing decision. Conversely, primary motor cortex is thought to execute planned movements indicating a completed decision by innervating muscles. Recent results question this strict division of labour among premotor and primary motor areas, but the exact role of primary motor areas in perceptual decision making remains unclear. Here we tested the hypothesis that human primary motor cortex follows the ups and downs of available evidence during decision making. We used stimuli changing randomly every 100 ms to induce fast variations in the available decision evidence throughout single trials. The stimuli were chosen such that participants had to observe typically more than 5 stimulus changes before being able to make a confident decision. This enabled us to investigate corresponding changes in brain signals within trials. We correlated the stimulus-induced varying evidence as predicted by an ideal observer model with the ongoing neuronal signals measured by magnetoencephalography. This approach provided us with unprecedented statistical precision for identifying brain areas that represent decision evidence. We found that the primary motor cortex of humans indeed represents decision evidence, at least 500 milliseconds before the actual response, confirming that it is not just executing, but also anticipating decisions.

Introduction

During perceptual decision making observers judge the state of their environment. Already while the observer makes the decision, brain areas presumably related to motor planning such as premotor cortex and the frontal eye fields represent evidence for the decision (Gold & Shadlen, 2007; Hanks & Summerfield, 2017). In contrast, primary motor cortex has traditionally been only associated with the execution of movements through the suitable activation of muscles (Kalaska & Rizzolatti, 2012). This view suggests that the primary motor cortex is only marginally involved in the decision making process by signalling the outcome of the decision in the form of a motor command.

This strict functional role of primary motor cortex as a motor control device has come under strain in the recent past. In monkeys, there are single primary motor cortex neurons whose firing rate appears to track the decision evidence shown on a screen before committing to a motor response (Thura & Cisek, 2014). In humans, lateralised oscillatory signals, for example, in the beta band measured with magnetoencephalography (MEG) exhibit choice predictive build-up that is thought to mirror the increasing evidence for a decision and the sources of these oscillations have been located in dorsal premotor and primary motor cortex (Donner, Siegel, Fries, & Engel, 2009). Lateralised readiness potentials and oscillations in the electroencephalogram (EEG) correlate with the average strength of evidence before the motor response (Kelly & O'Connell, 2013; Lange, Rahnev, Donner, & Lau, 2013) and are thought to originate in primary motor cortex (Smulders & Miller, 2012). Further, reflex gains in elbow muscles exhibit evidence-dependent build-up (Selen, Shadlen, & Wolpert, 2012). These findings suggest that also primary motor cortex prepares responses in proportion to the available evidence during decision making. The results in humans, however, are only based on indirect, average measures of decision evidence such as a general build-up of evidence within a trial (Donner et al., 2009), or the average strength of decision evidence within and across trials (Kelly & O'Connell, 2013; Lange et al., 2013; Selen et al., 2012).

A more direct approach to investigate representations of decision evidence in the brain is to control the amount of available evidence during decision making by manipulating the stimulus such that evidence fluctuates in specific patterns throughout an experimental trial instead of simply being constant or increasing steadily (Brunton, Botvinick, & Brody, 2013; Thura & Cisek, 2014; Wyart, Gardelle, Scholl, & Summerfield, 2012). The advantage of this approach, relative to previous ones, is that the induced evidence fluctuations enable more specific predictions about the time course of measured evidence signals and therefore increase the power and specificity of the corresponding analyses. Applying this approach to MEG measurements we, therefore, expected to be able to identify areas in the human brain that specifically represent decision evidence while the decision develops. Although the focus of our analyses was on primary motor cortex, the approach also allowed us to test for representations of decision evidence across the whole cerebral cortex.

Using source reconstruction of the MEG data, we found significant correlations with decision evidence in primary motor cortex 300 to 500 ms after the onset of a new stimulus element. Critically, these correlations were distinct from the motor signal related to a participant's actual motor response. This finding confirms that human primary motor cortex represents decision evidence while making perceptual decisions and not only executes decisions. Apart from primary motor cortex, we identified the posterior cingulate cortex as a brain area with consistent representations of decision evidence.

Results

While MEG was recorded, 34 human participants observed a single white dot on the screen changing its position every 100 ms and had to decide whether a left or a right target (two yellow dots) was the centre of the white dot movement (**Figure 1**). Participants indicated their choice with a button press using the index finger of the corresponding hand. The distance of the target dots on the screen was chosen in behavioural pilots so that participants had an intermediate accuracy around 75% while being told to be as accurate and fast as possible. The average median response time across participants was 1.1 s with an average accuracy of 78% (cf. **Figure 1**).

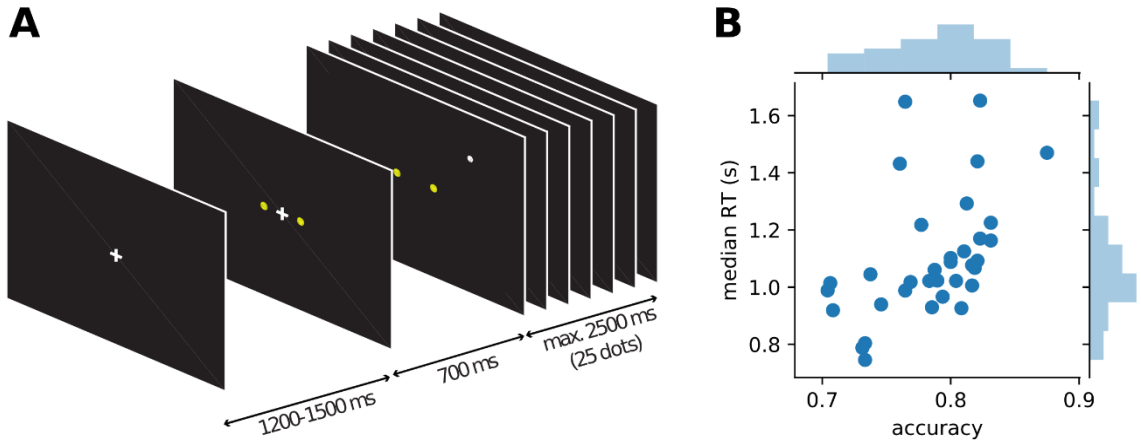

Figure 1. Course of events within a trial in the single dot task (A) and behaviour of individual participants (B). Each trial started with the presentation of a fixation cross, followed by the appearance of the two yellow targets after about 1 s. 700 ms after the appearance of the targets the fixation cross disappeared and a single white dot was presented at a random position on the screen (drawn from a 2D-Gaussian distribution centred on one of the targets). Every 100 ms the position of the white dot was changed to a new random draw from the same distribution. Participants were instructed to indicate the target which they thought was the centre of the observed dot positions. After 25 dot positions (2.5 s) without a response, a new trial was started automatically, otherwise a new trial started with the response of the participant. Average behaviour (accuracy and median response time) for each of the 34 participant is shown in B.

An ideal observer model for inference about the target given a sequence of single dots has been described before (Bitzer, Park, Blankenburg, & Kiebel, 2014; Park, Lueckmann, Kriegstein, Bitzer, & Kiebel, 2016). This model identifies the x-coordinates of the white dot positions as momentary decision evidence while the y-coordinate only provides irrelevant perceptual information and acts as a decision-unrelated control variable. Further, the sum of x-coordinates across single dot positions reflects accumulated evidence and corresponds to the average state of a discrete-time drift-diffusion model (Bitzer et al., 2014).

Participants integrate evidence provided by single dot positions to make decisions

As the task required and the model predicted, participants made their decision based on the provided evidence. In **Figure 2** we show this as the correlation of participants' choices with momentary and accumulated evidence. Momentary evidence was mildly correlated with choices throughout the trial (correlation coefficients around 0.3) while the correlation between accumulated evidence and choices increased to a high level (around 0.7) as more and more dot positions were presented. This result indicates that participants accumulated the momentary evidence, here the x-coordinate of the dot, to make their choices. In contrast, as expected, the y-coordinates had no influence on the participants' choices as indicated by correlation coefficients around 0 (**Figure 2**B).

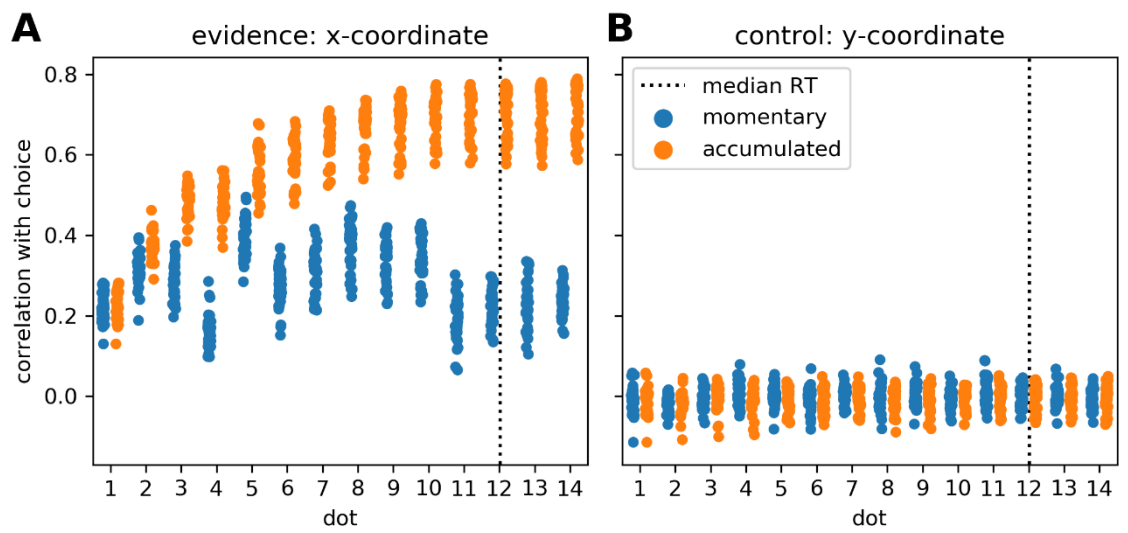

Figure 2. Participants accumulate momentary evidence provided by dot positions for making their decisions. (A) Each shown point corresponds to the Pearson correlation coefficient for the correlation between choices of a single participant and the sequence of presented dot positions across the 480 trials of the experiment. We plot, over stimulus duration, the momentary (blue) and the accumulated evidence (orange). The dotted vertical line shows the median RT across participants. Until about the 10th dot presentation the correlation between accumulated evidence and participant choices rises, reaching values around 0.7 while the momentary evidence is only modestly related to participant choices across all dots. **(B)** The same format as in A but all measures are computed from the y-coordinates of dot positions. As expected, y-coordinates do not correlate with participant choices.

Naturally, momentary and accumulated evidence can correlate quite strongly, because the last sampled x-coordinate has a strong influence on the accumulated evidence (**Supplementary Figure 1**). Therefore, we here only report results for momentary decision evidence and mean momentary evidence whenever writing "evidence" in the text unless stated explicitly otherwise. As **Figure 2** shows, and as expected, the momentary evidence is more clearly dissociated from the final choice of the participants than the accumulated evidence. This feature of the momentary evidence will be useful below in separating effects related to decision evidence from effects related to the final choice.

MEG signals correlate with evidence at specific time points after stimulus update

For the analysis of the MEG data we used regression analyses computing event-related regression coefficients (Clarke, Taylor, Devereux, Randall, & Tyler, 2013; Hauk, Davis, Ford, Pulvermüller, & Marslen-Wilson, 2006). For our main analysis the regressors of interest were the momentary evidence and y-coordinates of the dots. We normalised both the regressors and the data so that the resulting regression coefficients could be interpreted as approximate correlation values while accounting for potential covariates of no interest (see Methods). Note that this correlation analysis contrasts with standard event-related fields, where one would test for the presence of some constant time-course across trials. With the correlation analysis, the estimated regression coefficients describe how strongly the MEG signal, in each time point and each sensor (or source), followed the ups and downs of variables such as the momentary evidence, across trials.

As a first result, we found that correlations between momentary evidence and MEG signals followed a stereotypical temporal profile after each dot position update (cf. **Supplementary Figure 2**). Therefore, we performed an expanded regression analysis where we explicitly modelled the time from each dot position update, which we call 'dot onset' in the following. To exclude the possibility that effects signalling the button press motor response influence the results of the dot onset aligned analysis, we

only included data up until at least 200 ms prior to the participant response of each trial into this analysis.

We first identified time points at which the MEG signal correlated most strongly with the momentary evidence. To do this we performed separate regression analyses for each time point from dot onset, magnetometer sensor and participant, computed the mean regression coefficients across participants, took their absolute value to yield a magnitude and averaged them across sensors. **Figure 3** shows that the strongest correlations between decision evidence and magnetometer signals occurred at 120 ms, 180 ms and in a prolonged period from roughly 300 to 500 ms after dot onset. In contrast, correlations with the control, that is, the dot y-coordinates, were significantly lower in this period from 300 to 500 ms (two-tailed Wilcoxon test for absolute average coefficients across all sensors and times within 300-500 ms, $W = 382781$, $p << 0.001$).

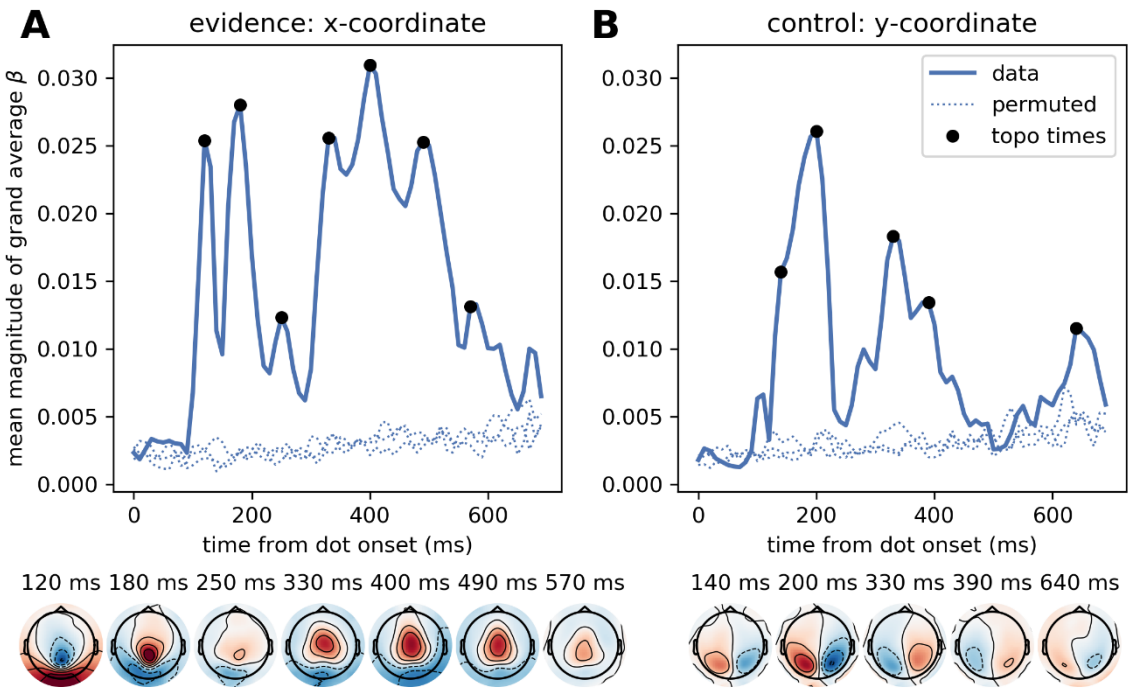

Figure 3. Time course of correlation strength with decision evidence and perceptual control variable. Top panels show time courses of the mean (across sensors) magnitude of grand average regression coefficients (β). For comparison, dotted lines show the corresponding values for data which were randomly permuted across trials before statistical analysis. Black dots indicate time points for which the sensor topography is shown below the plot. These topographies directly display the grand average regression coefficients at the indicated time with negative (blue) and positive (red) values. (**A**) The decision evidence has strong correlations with the magnetometer signal at 120 ms, 180 ms and from about 300 ms to 500 ms after dot onsets. (**B**) The y-coordinate correlations are visibly and significantly weaker than for the evidence, but there are two prominent peaks from about 120 ms to 210 ms and at 320 ms after dot onset. There is no sustained correlation with the y-coordinate beyond 400 ms and the topographies of magnetometers differ strongly between evidence and y-coordinates. Specifically, the evidence exhibits centro-parietal topographies whereas the y-coordinate exhibits strong correlations only in lateral occipito-parietal sensors.

The sensor topographies shown in **Figure 3** also indicate for the decision evidence a progression of the strongest correlations from occipital to central sensors while y-coordinate correlations remained spatially at occipito-parietal sensors.

A motor-posterior cingulate network of brain areas correlating with decision evidence

We reconstructed source currents along the cerebral cortex for each participant and subsequently repeated our regression analysis on the estimated sources. Specifically, we performed source reconstruction on the preprocessed MEG data using noise-normalised minimum norm estimation

based on all MEG sensors (Dale et al., 2000; Gramfort et al., 2013, 2014). Further, we aggregated estimated values by averaging across sources within 180 brain areas defined by a recently published brain atlas (Glasser et al., 2016). This resulted in average time courses for each experimental trial in each of the 180 brain areas defined per hemisphere for each participant. We then repeated the expanded regression analysis on these source-reconstructed time courses instead of on MEG sensors. Following the summary statistics approach we identified time points and areas with significant second-level correlations by performing t-tests across participants and applying multiple comparison correction using false discovery rate (Benjamini & Hochberg, 1995) simultaneously across all time points and brain areas.

In the time window from 300 to 500 ms after dot onset significant correlations with decision evidence occurred predominantly in bilateral primary motor, somatosensory and posterior cingulate cortices, as shown in **Figure 4**.

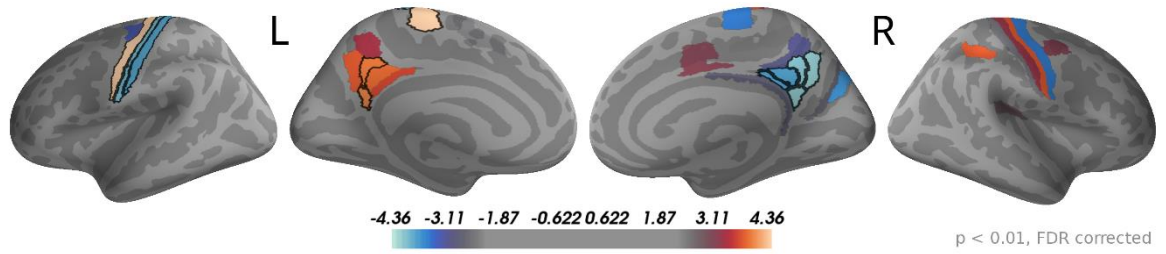

Figure 4. Primary motor, somatosensory and posterior cingulate cortices exhibit significant correlation with decision evidence in the time window of 300 to 500 ms after dot onset. Only brain areas with at least one significant correlation ($p < 0.01$, FDR corrected) within the time window are coloured. Colours show average second-level t-values where the average is taken over time points between 300 to 500 ms. The five areas with the strongest correlations (in that order) in the left hemisphere were (specified as Brodmann areas with subdivisions as defined in (Glasser et al., 2016); indicated by borders around areas): area 4, 3a, v23ab, 31pd, 3b and in the right hemisphere: v23ab, 7m, 31pd, 31pv, d23ab. All effects are listed in **Supplementary Table 2**.

Spatial pattern of correlations in motor cortex is similar to activation for response

Having established the involvement of primary motor and somatosensory cortices in representing the momentary evidence we tried to further clarify the nature of these effects. In a first step, we compared the found spatial pattern of correlations with the response-specific (button press) activations in motor areas. To do this we computed standard event-related averages centred on the response time of the participants in source space. Additionally, to provide for a high spatial resolution, we repeated the expanded regression analysis directly on sources of premotor and motor areas without averaging across sources within area. For the comparison of spatial patterns resulting from both analyses we selected those time points for each analysis which had the strongest effects in terms of second-level t-values in bilateral primary motor cortex (area 4). These time points were 490 ms after dot onset for the analysis centred on dot onset and 30 ms after the response for the response-aligned averages (cf. **Supplementary Figure 3**). The resulting spatial patterns are shown in **Figure 5** where one can see that the sources of both effects have the same location in dorsal premotor and primary motor cortex. Importantly, as we excluded in the dot onset centred analysis all time points earlier than 200 ms before the motor response, this result indicates that the areas in the brain that were involved in the execution of the button presses also represented decision-relevant information before the button press.

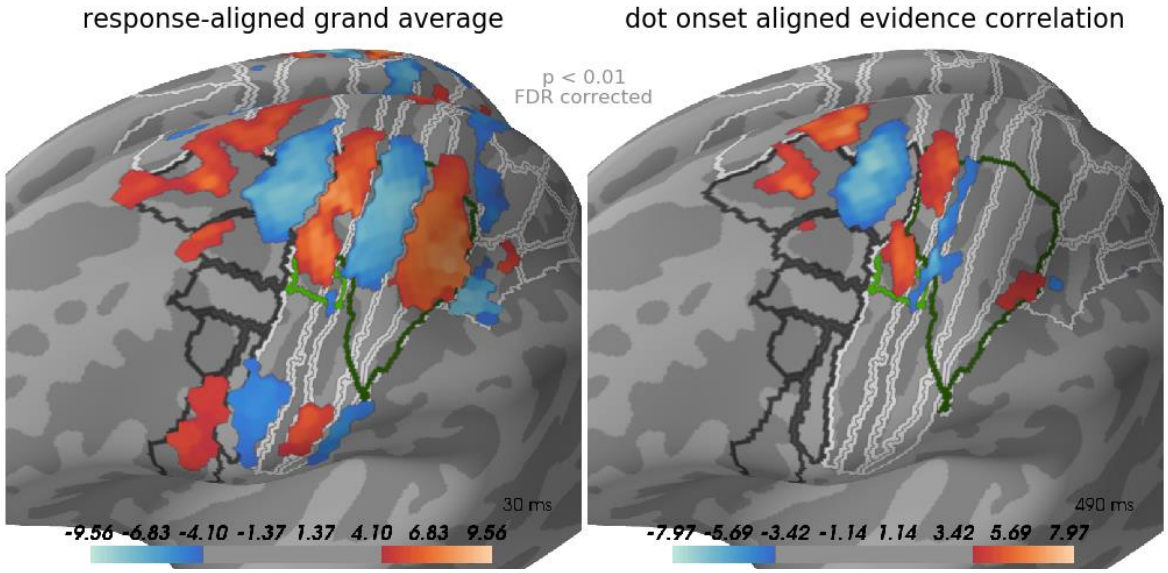

Figure 5. Spatial patterns of motor response-related effects and decision evidence correlations are similar. Spatial patterns of effects in premotor (dark outlines) and motor areas of the left hemisphere: (left) response-related grand averages at their peak times in primary motor cortex and (right) correlations with dot decision evidence. In both analyses colours indicate second-level t-values that were significant based on an FDR correction (across both time points and sources) at $\alpha = 0.01$. Although the response-related effects have higher t-values, the spatial patterns over dorsal premotor and primary motor cortex are rather similar despite the fundamental difference in data and analysis methods (see Methods for details). Green outlines: eye (light green) and upper limb (dark green) subregions of the sensorimotor strip defined in (Glasser et al., 2016).

Correlations with decision evidence in primary motor cortex occur well before the response

In the previous, dot onset aligned analyses we excluded all data of time points later than 200 ms before the response. This allowed us to exclude the possibility that response-related effects around the response time influenced the found effects. To further investigate how early before the response correlations with decision evidence occurred in primary motor cortex we conducted a response-aligned regression analysis. To increase the statistical power of the analysis, similar to the expanded regression analysis used above, we repeated the analysis for different assumed delays between a dot position update on the screen and the neural effect. We then averaged regression coefficients across delays from 300 to 500 ms within participant before conducting the second-level analysis. This means that an effect at time point -500 ms from the response reflects a correlation of the signal 500 ms before the response with dot positions that were visible on the screen 800 to 1000 ms before the response. See Methods for a detailed description of the procedure.

Figure 6 shows that there were significant correlations between the signal in primary motor cortex and decision evidence at least up to 500 ms and earlier before the response. Correlations with the control variable, the y-coordinate, fluctuated around 0 without significant effects at any time after multiple comparison correction. As expected, sources in left primary motor cortex showed large positive correlations in trials with large positive evidence (presented on the right half of the screen) while right primary motor cortex showed anti-correlation with evidence indicating large signal values in trials with large negative evidence (presented on the left half of the screen).

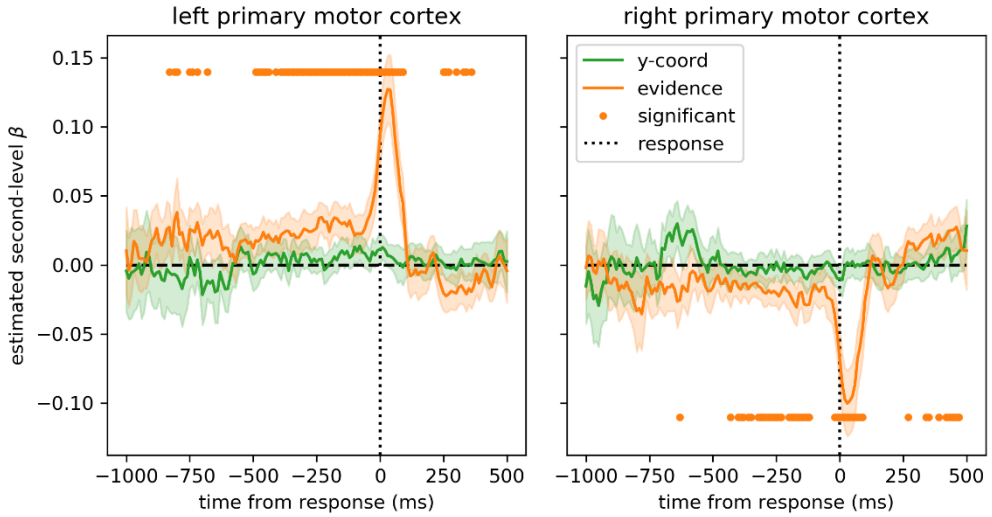

Figure 6. Correlations with decision evidence and dot y-coordinates in left and right primary motor cortex (area 4) aligned to response time. Strongest correlations with decision evidence (orange) occurred just after the response and can be attributed to response-related motor processes (see main text). However, evidence-correlations can be observed already 500 ms and earlier before the response. For comparison, y-coordinate-correlations are shown in green. Lines depict mean regression coefficients across participants together with a band of uncertainty showing twice the standard error of the mean (see Methods for details). Small coloured dots indicate time points at which the corresponding regressor differed significantly from 0 after multiple comparison correction for the number of time points across both hemispheres (FDR α = 0.01, no significant effects for the y-coordinate).

The peaks (orange line) just after the response (dotted line) in **Figure 6** reflect the motor response typically observed for primary motor cortex. Around these time points left primary motor cortex is strongly activated for a right button press and the right primary motor cortex is strongly activated for a left button press, but not the other way around. This is also reflected in corresponding peaks in the evoked signal (cf. **Supplementary Figure 3**). This motor response results in an increase in correlation with decision evidence, because i) on average the evidence provided by dot positions will point towards the correct choice, as expressed in the correlation between evidence and choice (cf. **Figure 2**) and ii) the motor response signal is rather strong such that it leads to a larger correlation with decision evidence as compared to pre-response time points.

Signals in posterior cingulate cortex correlate with decision evidence at early and late time points after dot onset

In addition to motor cortex our results in **Figure 4** identify the posterior cingulate cortex as another key brain region involved in representing decision evidence. While posterior cingulate cortex has been associated with perceptual decision making before (Heekeren, Marrett, Bandettini, & Ungerleider, 2004; Heekeren, Marrett, Ruff, Bandettini, & Ungerleider, 2006; Keuken et al., 2014; Philiastides, Heekeren, & Sajda, 2014; Tosoni, Galati, Romani, & Corbetta, 2008), its precise role during perceptual decision making is still mostly unclear. To further enquire this role we tested whether the signal in posterior cingulate cortex exhibits correlations with decision evidence outside the time window of 300 to 500 ms after dot onset as in **Figure 4**. We found significant correlations in posterior cingulate cortex already at 120 ms after dot onset, similarly as for early visual areas such as the primary visual cortex (**Supplementary Table 1**). Further, the signal in posterior cingulate cortex exhibited correlations with decision evidence around 180 ms after dot onset (cf. **Figure 7**), although these did not become significant after correcting for multiple comparisons across the shown time points and brain areas (in **Figure 7**A and B).

Among the effects in posterior cingulate cortex, area v23ab (roughly the ventral part of BA 23) stands out, because it consistently exhibited relatively strong correlations (magnitude of second-level t-values > 2) with decision evidence at the three time periods 120 ms, 180 ms, and 300 to 500 ms after dot onset (**Figure 7**B). In general, the time course of the correlation strength followed that of the grand average shown in **Figure 3**A, but the sign of the correlation switched between 120 and 180 ms (**Figure 7**B). This means that initially the signal in area v23ab increased for dot positions shown on the ipsilateral side of the screen while at later time points we observed larger signals for dot positions on the contralateral side.

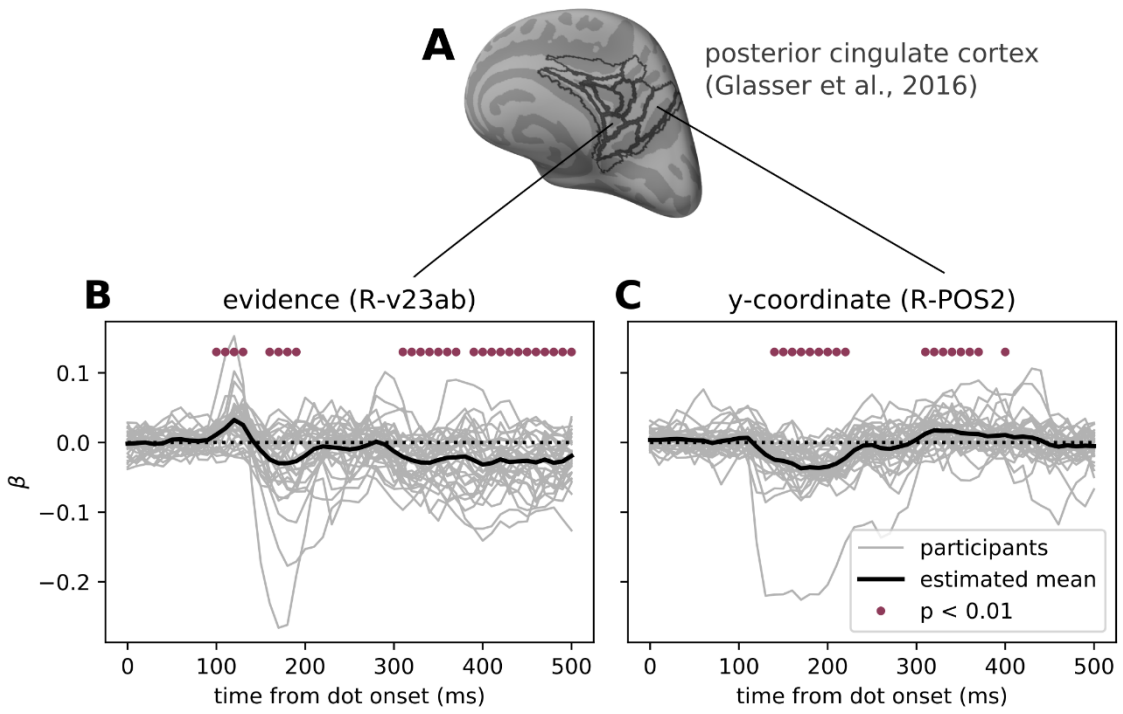

Figure 7. Areas in posterior cingulate cortex track dot position changes throughout the first 500 ms after dot onset. (**A**) Areas in posterior cingulate cortex (dark outlines) in right hemisphere as defined in (Glasser et al., 2016) shown in a medial view of the inflated cerebral cortex. For the decision evidence (**B**) and y-coordinate (**C**) we selected the brain areas with the highest mean absolute correlations across time from dot onset. These were both located in posterior cingulate cortex (evidence: right v23ab, y-coordinate: right POS2). The panels show time courses for the corresponding regression coefficients (β) for individual participants (light grey) and their second-level mean (black). Dots above the traces indicate time points at which the second-level mean differed significantly from 0 ($p < 0.01$, uncorrected).

For the perceptual control variable, the y-coordinate, an area in posterior cingulate cortex exhibited the strongest correlations across time from dot onset (right POS2). However, these correlations were relatively small after about 220 ms and specifically after 400 ms from dot onset and generally followed the corresponding time course of the whole-brain correlation strength shown in **Figure 3**.

Discussion

We have investigated the involvement of motor areas in the human brain during a perceptual decision making task. In contrast to previous studies (Donner et al., 2009; Kelly & O'Connell, 2013; Lange et al., 2013), we directly examined in how far brain signals as measured with MEG correlate with fast changes in the available decision evidence. We induced these fast evidence fluctuations using a visual stimulus in which new evidence appeared every 100 ms. Motor areas and specifically primary motor cortex exhibited correlations with individual pieces of decision evidence 300 to 500 ms after the new evidence appeared on the screen. These correlations in primary motor cortex could be distinguished from the

motor response and occurred several hundreds of milliseconds before the actual response. These results, therefore, confirm that the human primary motor cortex does not merely execute completed decisions, but also prepares motor responses in proportion to the available decision evidence. Apart from motor areas we additionally found posterior cingulate cortex to represent decision evidence. While the correlations with evidence occurred in motor cortex only in the time window from 300 to 500 ms post-stimulus, correlations in posterior cingulate cortex occurred additionally already at 120 and 180 ms.

To manipulate decision evidence in our task we changed the position of a single dot presented on a screen. Only the x-coordinates of these dot positions represented decision evidence while the decision-irrelevant y-coordinates acted as a perceptual control variable. We have shown that correlations of brain signals with the perceptual control variable, in contrast to decision evidence, were strongly diminished in the period from 300 to 500 ms after dot onset. This suggests that the brain ceases to represent perceptual information that is behaviourally irrelevant around this time and that brain areas with strong correlations with decision evidence in this time window indeed are involved in decision making. This interpretation is further supported by previous work which has shown that purely perceptual stimulus information is represented in electrophysiological signals only until about 400 ms after stimulus onset (Mostert, Kok, & Lange, 2015; Myers et al., 2015; Wyart et al., 2012) while specifically decision-related information is represented longer starting around 170 ms after stimulus onset (Mostert et al., 2015; Myers et al., 2015; Philiastides et al., 2014; Philiastides, Ratcliff, & Sajda, 2006; Philiastides & Sajda, 2006; Wyart et al., 2012).

Although previous work has already pointed towards the possibility that the primary motor cortex of primates represents decision evidence in certain situations (Donner et al., 2009; Thura & Cisek, 2014; Tosoni et al., 2008), the present results support this conjecture for the human brain in unprecedented precision. Specifically, we were able to show that human primary motor cortex not only increases its activity in preparation for a response, as, for example, measured in lateralised readiness potentials (Smulders & Miller, 2012), or shown for a motion discrimination task (Donner et al., 2009), but the average source currents in primary motor cortex tend to rise and fall with decision evidence on a timescale of 100 ms. According to our results, these decision evidence signals in primary motor cortex are about an order of magnitude weaker than the response-related signal in primary motor cortex (cf. **Figure 6** pre-response correlations versus post-response peak).

One potential caveat of our correlation results in primary motor cortex is: Could it be that we only observed evidence correlations in primary motor cortex, because participants actually executed micro-movements that tried to track the perceptual stimulus? Especially, did participants try to follow dot movements on the screen with their eyes, or did their fingers slightly move over the corresponding buttons, when the dot was shown on the respective side of the screen? Although we cannot completely exclude this possibility we deem it unlikely, because: i) Dots were shown only very centrally at visual angles within about 10° visual angle with most dots within 5° diameter from fixation meaning that most dots were well within the foveal visual field. ii) The spatial pattern of early evidence correlations corresponds to that of later button press responses (**Figure 5**), that is, it does not appear to be specifically related to eye movements. iii) Other pre-response motor effects have been reported in the EEG in tasks with stimuli which did not change their location within a trial and therefore could not prompt decision-unrelated movements towards the corresponding side during decision making (Donner et al., 2009; Gould, Nobre, Wyart, & Rushworth, 2012; Kelly & O'Connell, 2013; Lange et al., 2013). In conclusion, we do not believe that the correlations with decision evidence observed in primary motor cortex are merely an expression of motor control signals that caused stimulus-correlated micro-movements. Even if such micro-movements existed, we deem it likely that these follow the time-course

of decision evidence rather than decision-irrelevant stimulus properties, as suggested by recent results about the adaptation of reflex gains during decision making (Selen et al., 2012).

What is the functional role of primary motor cortex, beyond its obvious role of causing the movement? The present results support the notion that primary motor cortex continuously prepares for the execution of alternative actions in proportion to their behavioural relevance before committing to a choice, as it has been found for single neurons in monkeys (Thura & Cisek, 2014). Such an interpretation would be congruent with the affordance competition hypothesis (Cisek, 2007) which describes movement generation as a dynamic process in which possible actions compete with each other and are continuously refined in a loop between sensory and motor related areas while frontal areas provide contextual modulation.

Given that primary motor cortex itself, as the area in cerebral cortex that is most directly associated with the execution of movements, represents decision evidence, one may ask whether the eventual choice is also made in primary motor cortex and not, for example, in more frontal regions. Possible neural implementations of a suitable mechanism have been proposed (Wang, 2008). In these, different pools of neurons in one brain area compete until a threshold is crossed and one pool decisively signals the choice. Our results are compatible with such a mechanism, but one can ultimately not exclude the possibility that the decision is formed somewhere else in the brain and primary motor cortex only represents the results of this process. We also observed some correlations with decision evidence in premotor regions (**Figure 4** and **Figure 5**), but these tended to be weaker than in primary motor cortex (**Supplementary Table 2**). We did not find any correlations of sufficient strength to pass the correction for multiple comparisons in other frontal areas (**Supplementary Table 1**). Although this may suggest that primary motor cortex plays a more important role in the decision making process than these areas, the lack of correlation may also be explained by the sensitivity profile of MEG measurements across cerebral cortex. It has, for example, previously been noted that "only areas with a macroscopic contralateral motor bias were apt to signal subjects' choices", when measured with MEG (Donner et al., 2009). That we were able to identify additional areas representing decision evidence, specifically the posterior cingulate cortex, supports the strength and increased power of our approach compared to previous ones, but the precise limits of which representations of decision evidence in the brain can and cannot be detected with MEG has still to be determined.

Based on single neuron recordings in dorsal premotor cortex, primary motor cortex and the basal ganglia of monkeys, it has been suggested that perceptual decisions are made in premotor or primary motor cortex while the basal ganglia eventually invigorate the movement selected in motor cortex (Thura & Cisek, 2017). While these findings, as ours, have been obtained with perceptual decision making tasks in which sensory evidence immediately maps to a button press or reaching movement, it is an interesting future research question how representations of evidence across motor areas change, when the response mapping is only revealed after the decision, for example with a sufficiently large delay after the offset of stimulus presentation (Filimon, Philiastides, Nelson, Kloosterman, & Heekeren, 2013; Liu & Pleskac, 2011). In this situation the brain cannot frame decision making as a competition between specific actions and may represent decision evidence in different coordinates and in different brain areas than primary motor cortex.

The correlations found in posterior cingulate cortex rivalled in strength those of primary motor cortex, or even exceeded it (**Supplementary Table 2**). Further, while in motor areas these correlations occurred only from about 300 ms after the evidence first became available, we also observed significant correlations much earlier, around 120 ms and 180 ms, in posterior cingulate cortex and specifically in the ventral part (**Figure 7**). We speculate that the first time point of significant correlations around 120 ms reflects early sensory processing of dot positions, because we found the by far largest effects at this

time point in early visual areas such as primary visual cortex (**Supplementary Table 1**). From about 180 ms after stimulus onset, however, it has been found that information about the decision can be decoded from brain signals (Lange, Jensen, & Dehaene, 2010; Mostert et al., 2015; Myers et al., 2015; Philiastides et al., 2006; Philiastides & Sajda, 2006). This suggests that these later effects may represent processes directly involved in forming the decision. Consequently, posterior cingulate cortex appears to be involved in both early sensory processing and decision making and, therefore, could act as a bridge between these processes.

Previous studies investigating the function of posterior cingulate cortex have mostly concentrated on slow time scales, for example, contrasting different task conditions to each other, while we analysed rapid fluctuations of neural signals. These investigations of slow changes in posterior cingulate cortex activations have identified the posterior cingulate as a key node in the default mode network which deactivates as attention is focused on external stimuli (Leech & Sharp, 2014). However, posterior cingulate cortex has been associated with a wide range of functions which have recently been proposed to be consolidated as estimating the need to change behaviour in light of new, external requirements (Pearson, Heilbronner, Barack, Hayden, & Platt, 2011). Our findings are compatible with this view, when transferred to the context of comparably fast perceptual decision making where decision evidence may be viewed as the need to follow one or another behaviour.

In summary, our findings suggest that during perceptual decision making posterior cingulate cortex is involved in transforming sensory signals into behaviourally relevant information. This information is shared with primary motor cortex which continuously prepares the corresponding actions in proportion to the available evidence.

Materials and Methods

This study has been approved by the ethics committee of the Technical University of Dresden (EK324082016). Written informed consent was obtained from all participants.

Participants

37 healthy, right-handed participants were recruited from the Max Planck Institute for Human Cognitive and Brain Sciences (Leipzig, Germany) participant pool (age range: 20 – 35 years, mean 25.7 years, 19 females). All had normal or corrected-to-normal vision, and reported no history of neurologic or psychiatric disorders. One participant was excluded from MEG measurement due to low performance during training. In total, 36 participants participated in the MEG study. Two participants' data were excluded from analyses due to excessive eye artefacts and too many bad channels. Finally, 34 participants' data were analysed.

Stimuli

In each trial, a sequence of up to 25 white dots were presented on a black screen. Each dot was displayed for 100 ms (6 frames, refresh rate 60 Hz). The white dot was located at x, y coordinates which were sampled from one of two two-dimensional Gaussian distributions with means located at ±25 pixels horizontal distance from the centre of the screen. The standard deviation was 70 pixels in both axes of the screen. The mean locations were the two target locations (-25: left, 25: right). These target locations corresponded to visual angles ±0.6° from the centre of the screen. The standard deviation of the Gaussian distribution corresponded to ±1.7° from the two target locations. The stimuli used in this study consisted of a subset of stimuli used previously (Park et al., 2016), and additional newly created stimuli. The stimuli were chosen to increase the probability that the participants see the 5th dot within the 25 dot sequence by not responding earlier. In short, trials where ~70% of the participants in the Park et al. study had reaction times (RT) longer than 700 ms but not timed-out were chosen from the

second most difficult condition. This resulted in 28 trials from 200 trials. Then each trial was copied 6 times, with only the 5th dot location differing, ranging in 'target location + [-160 -96 -32 32 96 160] (pixels)'. This resulted in 168 trials. These trials were mirrored to create a dataset with the same evidence strengths but with different x coordinate signs (336 trials), and finally trials which had short RTs were chosen from (Park et al., 2016) as catch trials, to prevent participants from adapting to the long RT trials (30% of the total trials). This resulted in a total of 480 trials per experiment.

We originally designed this stimulus set, especially the manipulations of the 5th dot, to increase the chance of inducing sufficiently large effects in the MEG signal when observing the 5th dot. In a preliminary analysis we realised, however, that the natural variation of the stimuli already induces observable effects. Consequently, we pooled all trials for analysis.

Procedure

Participants were seated in a dimly lit shielding room during the training and the MEG measurement. Visual stimuli were presented using Presentation® software (Version 16.0, Neurobehavioral Systems, Inc., Berkeley, CA, www.neurobs.com). The display was a semi-transparent screen onto which the stimuli were back-projected from a projector located outside of the magnetic shielding room (Vacuumschmelze Hanau, Germany). The display was located 90 cm from the participants. The task was to find out which target (left or right) was the centre of the white dot positions, but participants were instructed with a cover story: Each target represented a bee hive and the white dot represented a bee. Participants should tell which bee hive is more likely the home of the bee. They were additionally instructed to be both accurate and fast, but not too fast at the expense of being inaccurate, and not too slow that the trial times out. They went through a minimum 210 and maximum 450 trials of training, until they reached a minimum of 75% accuracy. Feedback (correct, incorrect, too slow, too fast) was provided during the training. After training, a pseudo-main block with 200 trials without feedback preceded MEG measurement. After the pseudo-main session, the 480 trials in randomized order were presented to each participant divided into 5 blocks. The MEG measurement lasted ~ 60 minutes, including breaks between blocks. Each trial started with a fixation cross (randomized, 1200 ms ~ 1500 ms uniform distribution) followed by two yellow target dots. After 700 ms, the fixation cross disappeared and the first white dot appeared. The white dot jumped around the screen and stayed at each location for 100 ms, until the participant submitted a response by pressing a button using either hand, corresponding to the left / right target, or when the trial timed-out (2.5 s). In order to maintain motivation and attention throughout the measurement, participants were told to accumulate points (not shown to the participants) for correct trials and adequate (not too slow and not too fast, non-time-out) RTs. Bonus money in addition to compensation for participating in the experiment were given to participants with good performances. RTs and choices were collected for each trial for each participant. Although the trial order was randomized across participants, every participant saw exactly the same 480 trials.

MEG data acquisition and preprocessing

MEG data were recorded with a 306 channel Vectorview device (Elekta Oy, Helsinki, Finland), sampled at 1000 Hz. The MEG sensors covered the whole head, with triplet sensors consisting of two orthogonal gradiometers and one magnetometer at 102 locations. Additionally, three electrode pairs were used to monitor eye movement and heart beats at the same sampling rate. The raw MEG data was corrected for head movements and external interferences by the Signal Space Separation (SSS) method (Taulu, Simola, & Kajola, 2005) implemented in the MaxFilterTM software (Elekta Oy) for each block. The subsequent preprocessing was performed using MATLAB (Mathworks, Massachusetts, United States). The head movement corrected data was high-pass and low-pass filtered using a linear phase FIR Kaiser filter (corrected for the shift) at cut-off frequencies of 0.33 Hz and 45 Hz respectively, with filter orders

of 3736 and 392, respectively. The filtered data was then down-sampled to 250 Hz. Then independent component analysis (ICA) was applied to the continuous data using functions in the EEGLAB (Delorme & Makeig, 2004) to remove eye and heart beat artefacts. The data dimensionality was reduced by principal component analysis to 50 or 60 components prior to running the ICA. Components which had high temporal correlations (> 0.3) or typical topographies with/of the EOG and ECG signals were identified and excluded. The ICA-reconstructed data for each block was combined, and epoched from – 300 ms to 2500 ms from the first dot onset (zero). Another ICA was applied to these epoched data in order to check for additional artefacts and confirm typical neural topographies from the components. The ICA reconstructed data and original data were compared and inspected in order to ensure only artefactual trials were excluded. Before statistical analysis we used MNE-Python v0.15.2 (Gramfort et al., 2013, 2014) to downsample the data to 100 Hz (10 ms steps) and perform baseline correction for each trial where the baseline value was the mean signal in the period from -300 ms to 0 ms (first dot onset).

Source reconstruction

We reconstructed the source currents underlying the measured MEG signals using noise-normalised minimum norm estimation (Dale et al., 2000) implemented in the MNE software. To create participant-specific forward models we semi-automatically co-registered the head positions of participants with the MEG coordinate frame while at the same time morphing the participants' head shape to that of Freesurfer's fsaverage by aligning the fsaverage head surface to a set of head points recorded for each participant. We defined a source space along the white matter surface of the average subject with 4098 equally spaced sources per hemisphere and an approximate source spacing of about 5 mm (MNE's "oct6" option). For minimum norm estimation we assumed a signal-to-noise ratio of 3 (lambda2 = 0.11). We estimated the noise covariance matrix for noise normalisation (Dale et al., 2000) from the MEG signals in the baseline period spanning from 300 ms before to first dot onset in each trial. We further used fixed orientation constraints assuming that sources are normal to the cortical mantle and employed standard depth weighting with a value of 0.8 to overcome the bias of minimum norm estimates towards superficial sources. We computed the inverse solution from all MEG sensors (magnetometers and the two sets of gradiometers) returning dynamic statistical parametric maps for each participant. Before some of the subsequent statistical analyses we averaged the reconstructed source signals across all sources of a brain area as defined by the recently published HCP-MMP parcellation of the human connectome project (Glasser et al., 2016).

Regression analyses

Most of our results were based on regression analyses with a general linear model giving event-related regression coefficients (Clarke et al., 2013; Hauk et al., 2006). We differentiate between a standard regression analysis on events aligned at the time when the white dot appeared in each trial, expanded regression analyses on events aligned at the times of white dot position changes and response-aligned regression analyses.

Standard regression analysis

In the standard regression analysis we defined dot-specific regressors with values changing only across trials. For example, we defined a regressor for decision evidence (x-coordinate) of the 2nd white dot position presented in the trial. For convenience we also call white dot positions (1st, 2nd and so forth in the sequence of dot positions) simply 'dots'.

We only report results of a standard regression analysis in **Supplementary Figure 2**. This analysis included the dot x- and y-coordinates of the first 6 dots as regressors of interest (together 12 regressors). Additional nuisance regressors were: the response of the participant, a participant-specific

trial count roughly measuring time within the experiment, an intercept capturing average effects and a response entropy. The latter quantified the posterior uncertainty of a probabilistic model of the responses (Park et al., 2016) that the model had about the response for the stimulus presented in that trial after model parameters were adapted to fit participant responses. Specifically, the wider and flatter the posterior predictive distribution over responses of the model for a particular trial / dot position sequence was, the larger was the response entropy for that trial. The data for this analysis were the preprocessed magnetometer time courses.

Expanded regression analyses

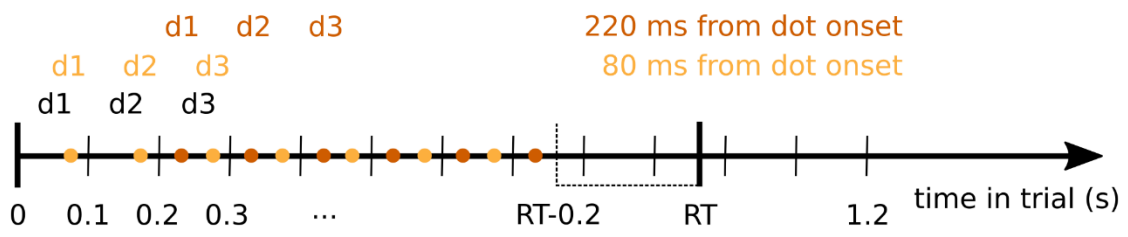

Figure 8. Diagram demonstrating the selection of data points entering the expanded regression analyses. Dot positions (d1, d2, d3, …) changed every 100 ms in the experiment (black). Coloured dots indicate times at which signal data points entered the analysis for a given time from dot position change (dot onset, shown exemplarily for 80 and 220 ms from dot onset). We only considered time points up to 200 ms before the response in each trial. Coloured d1, d2, d3 above the points indicate the dot positions associated with the corresponding signal data points for the given time from dot onset. For each trial, these pairs of signal data and dot positions entered the expanded regression analyses.

Expanded regression analyses were based on an expanded set of data created by dividing up the data into partially overlapping epochs centred on the times of dot position changes. For each time point after this dot onset the data contained a variable number of time points depending on how many more dots were presented in each individual trial before a response was given by the participant. For example, if a participant made a response after 880 ms in a trial, 9 dots were shown in that trial (onset of the 9th dot was at 800 ms). If we are interested in the time point 120 ms after dot onset (dot position change), this gives us 8 time points within that trial that were 120 ms after dot onset. Further excluding all time points 200 ms before the response and later, would leave us with 6 data points for this example trial. See **Figure 8** for an illustration. For each time after dot onset and for each participant we pooled all of these data points across trials and inferred regression coefficients on these expanded data sets. Note that this approach can equally be interpreted as statistical inference over how strongly the sequence of momentary evidence caused by the dot updates is represented in the signal at 100 ms wide steps with a delay given by the chosen time from dot onset.

These analyses included two regressors of interest: decision evidence (x-coordinate) and y-coordinate of the associated dots. We additionally included the following nuisance regressors: an intercept capturing average effects, the absolute values of x- and y-coordinates, perceptual update variables for x- and y-coordinates (Wyart et al., 2012) defined as the magnitude of the change from one dot position to another and accumulated values of x- and y-coordinates. Because we found that the accumulated values can be strongly correlated with the individual x- and y-coordinates (cf. **Supplementary Figure 1**), we only used accumulated values up to the previous dot in the regressor. For example, if a data point was associated with the y-coordinate of the 4th dot, the accumulated regressor would contain the sum of only the first three y-coordinates. This accumulated regressor is equal to the regressor resulting from Gram-Schmidt orthonormalisation of the full sum of y-coordinates with respect to the last shown y-coordinate. The accumulated evidence regressor was derived from the ideal observer model as the log posterior odds of the two alternatives, but this was almost 100% correlated with the simple sum of x-

coordinates. The small differences between model-based accumulated evidence and sum of x-coordinates after normalisation resulted from a small participant-specific offset representing the overall bias of the participant towards one decision alternative.

Identification of significant source-level effects

To identify significant correlations between regressors of interest and source signals we followed the summary statistics approach (Friston, Ashburner, Kiebel, Nichols, & Penny, 2006) and performed two-sided t-tests on the second level (group-level, t-tests across participants). We corrected for multiple comparisons across time points and brain areas by controlling the false discovery rate using the Benjamini-Hochberg procedure (Benjamini & Hochberg, 1995). Specifically, for identifying significant effects reported in **Figure 4** we corrected across 25,340 tests covering 70 time points (0 to 690 ms from dot onset in 10 ms steps) and 362 brain areas (180 brain areas of interest per hemisphere plus one collection of sources per hemisphere that fell between the area definitions provided by the atlas). We report all significant effects of this analysis in **Supplementary Table 1**.

Response-aligned analysis

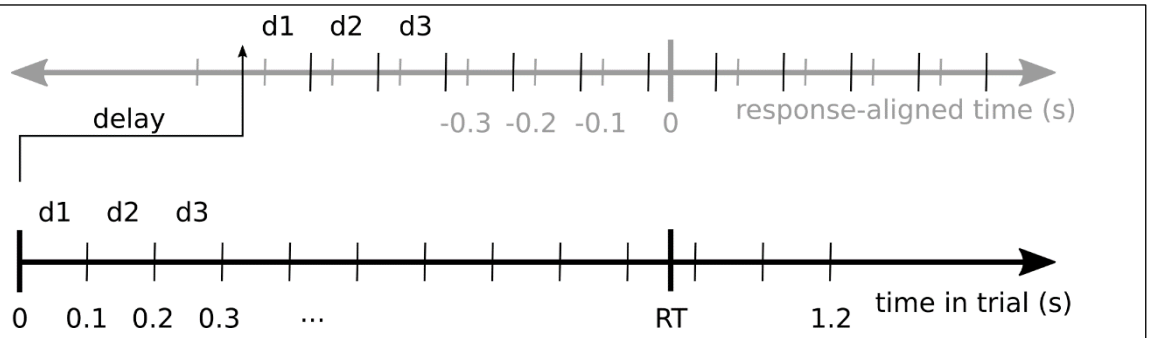

Figure 9. Diagram demonstrating standard and response aligned timings including considered delay for when correlations with a particular dot position (d1, d2, …) are expected.

In **Figure 6** we report time courses of group-level regression coefficients aligned to trial-specific response times of participants. To estimate the impact of dot positions on the signal in primary motor cortex (area 4) we associated each time point from the response in a trial with the dot position that was visible on the screen a fixed temporal distance (delay, **Figure 9**) before that time point. This delay implemented a hypothesis of when after a dot position change we would observe the effects in the signal in the form of correlations. For each time point from the response and participant and given a fixed delay we estimated regression coefficients for regressors x-coordinate, y-coordinate, perceptual updates for x and y and intercept across trials of individual participants. We further repeated this for all delays from 300 to 500 ms, because of our previous finding that evidence correlations were strong on average across the brain in this time period after dot onset. We then averaged regression coefficients across delays within participants, thus considering participant-level variation. We computed group-level statistics using two-sided t-tests over the averaged coefficients and corrected for multiple comparisons across time points and the two hemispheres with the Benjamini-Hochberg procedure with $\alpha = 0.01$. After this correction, only the evidence and intercept (response-aligned average) had group-level coefficients significantly different from 0 (evidence effects shown in **Figure 6**, significant intercept effects: 10-50 ms in left M1, -420 ms in right M1). **Figure 6** depicts the mean coefficients across participants for each time point before the trial-specific response together with a band of uncertainty with a width of twice the standard error of the mean above and below the mean.

Acknowledgements

We would like to thank Yvonne Wolff-Rosier for helping with data acquisition.

Competing interests

The authors declare that no competing interests exist.

References

Benjamini, Y., & Hochberg, Y. (1995). Controlling the false discovery rate: a practical and powerful approach to multiple testing. *Journal of the Royal Statistical Society. Series B. Methodological*, *57*(1), 289–300. Retrieved from http://www.jstor.org/stable/2346101

Bitzer, S., Park, H., Blankenburg, F., & Kiebel, S. J. (2014). Perceptual decision making: Drift-diffusion model is equivalent to a Bayesian model. *Frontiers in Human Neuroscience*, *8*(102). doi:10.3389/fnhum.2014.00102

Brunton, B. W., Botvinick, M. M., & Brody, C. D. (2013). Rats and humans can optimally accumulate evidence for decision-making. *Science*, *340*(6128), 95–98. doi:10.1126/science.1233912

Cisek, P. (2007). Cortical mechanisms of action selection: the affordance competition hypothesis. *Philosophical transactions of the Royal Society of London. Series B, Biological sciences*, *362*(1485), 1585–1599. doi:10.1098/rstb.2007.2054

Clarke, A., Taylor, K. I., Devereux, B., Randall, B., & Tyler, L. K. (2013). From perception to conception: how meaningful objects are processed over time. *Cerebral cortex (New York, N.Y. : 1991)*, *23*(1), 187–197. doi:10.1093/cercor/bhs002

Dale, A. M., Liu, A. K., Fischl, B. R., Buckner, R. L., Belliveau, J. W., Lewine, J. D., & Halgren, E. (2000). Dynamic statistical parametric mapping: combining fMRI and MEG for high-resolution imaging of cortical activity. *Neuron*, *26*(1), 55–67. doi:10.1016/S0896-6273(00)81138-1

Delorme, A., & Makeig, S. (2004). EEGLAB: an open source toolbox for analysis of single-trial EEG dynamics including independent component analysis. *Journal of neuroscience methods*, *134*(1), 9–21. doi:10.1016/j.jneumeth.2003.10.009

Donner, T. H., Siegel, M., Fries, P., & Engel, A. K. (2009). Buildup of choice-predictive activity in human motor cortex during perceptual decision making. *Curr Biol*, *19*(18), 1581–1585. doi:10.1016/j.cub.2009.07.066

Filimon, F., Philiastides, M. G., Nelson, J. D., Kloosterman, N. A., & Heekeren, H. R. (2013). How embodied is perceptual decision making? Evidence for separate processing of perceptual and motor decisions. *J Neurosci*, *33*(5), 2121–2136. doi:10.1523/JNEUROSCI.2334-12.2013

Friston, K. J., Ashburner, J. T., Kiebel, S. J., Nichols, T. E., & Penny, W. D. (Eds.). (2006). *Statistical Parametric Mapping: The Analysis of Functional Brain Images*. Academic Press. Retrieved from https://www.elsevier.com/books/statistical-parametric-mapping-the-analysis-of-functional-brain-images/penny/978-0-12-372560-8

Glasser, M. F., Coalson, T. S., Robinson, E. C., Hacker, C. D., Harwell, J., Yacoub, E., Ugurbil, K., et al. (2016). A multi-modal parcellation of human cerebral cortex. *Nature*, *536*(7615), 171–178. doi:10.1038/nature18933

Gold, J. I., & Shadlen, M. N. (2007). The neural basis of decision making. *Annu Rev Neurosci*, *30*, 535–574. doi:10.1146/annurev.neuro.29.051605.113038

Gould, I. C., Nobre, A. C., Wyart, V., & Rushworth, M. F. S. (2012). Effects of decision variables and intraparietal stimulation on sensorimotor oscillatory activity in the human brain. *J Neurosci*, *32*(40), 13805–13818. doi:10.1523/JNEUROSCI.2200-12.2012

Gramfort, A., Luessi, M., Larson, E., Engemann, D. A., Strohmeier, D., Brodbeck, C., Goj, R., et al. (2013). MEG and EEG data analysis with MNE-Python. *Frontiers in neuroscience*, *7*, 267. doi:10.3389/fnins.2013.00267

Gramfort, A., Luessi, M., Larson, E., Engemann, D. A., Strohmeier, D., Brodbeck, C., Parkkonen, L., et al. (2014). MNE software for processing MEG and EEG data. *NeuroImage*, *86*, 446–460. doi:10.1016/j.neuroimage.2013.10.027

Hanks, T. D., & Summerfield, C. (2017). Perceptual Decision Making in Rodents, Monkeys, and Humans. *Neuron*, *93*(1), 15–31. doi:10.1016/j.neuron.2016.12.003

Hauk, O., Davis, M. H., Ford, M., Pulvermüller, F., & Marslen-Wilson, W. D. (2006). The time course of visual word recognition as revealed by linear regression analysis of ERP data. *NeuroImage*, *30*(4), 1383–1400. doi:10.1016/j.neuroimage.2005.11.048

Heekeren, H. R., Marrett, S., Bandettini, P. A., & Ungerleider, L. G. (2004). A general mechanism for perceptual decision-making in the human brain. *Nature*, *431*(7010), 859–862. doi:10.1038/nature02966

Heekeren, H. R., Marrett, S., Ruff, D. A., Bandettini, P. A., & Ungerleider, L. G. (2006). Involvement of human left dorsolateral prefrontal cortex in perceptual decision making is independent of response modality. *Proc Natl Acad Sci U S A*, *103*(26), 10023–10028. doi:10.1073/pnas.0603949103

Kalaska, J. F., & Rizzolatti, G. (2012). Voluntary Movement: The Primary Motor Cortex. In E. R. Kandel, J. H. Schwartz, T. M. Jessell, S. A. Siegelbaum, & A. J. Hudspeth (Eds.), *Principles of Neural Science* (Fifth Edition.). McGraw-Hill Education.

Kelly, S. P., & O'Connell, R. G. (2013). Internal and external influences on the rate of sensory evidence accumulation in the human brain. *J Neurosci*, *33*(50), 19434–19441. doi:10.1523/JNEUROSCI.3355-13.2013

Keuken, M. C., Müller-Axt, C., Langner, R., Eickhoff, S. B., Forstmann, B. U., & Neumann, J. (2014). Brain networks of perceptual decision-making: an fMRI ALE meta-analysis. *Frontiers in human neuroscience*, *8*, 445. doi:10.3389/fnhum.2014.00445

Lange, F. P. de, Jensen, O., & Dehaene, S. (2010). Accumulation of evidence during sequential decision making: the importance of top-down factors. *J Neurosci*, *30*(2), 731–738. doi:10.1523/JNEUROSCI.4080-09.2010

Lange, F. P. de, Rahnev, D. A., Donner, T. H., & Lau, H. (2013). Prestimulus oscillatory activity over motor cortex reflects perceptual expectations. *J Neurosci*, *33*(4), 1400–1410. doi:10.1523/JNEUROSCI.1094-12.2013

Leech, R., & Sharp, D. J. (2014). The role of the posterior cingulate cortex in cognition and disease. *Brain : a journal of neurology*, *137*(Pt 1), 12–32. doi:10.1093/brain/awt162

Liu, T., & Pleskac, T. J. (2011). Neural correlates of evidence accumulation in a perceptual decision task. *J Neurophysiol*, *106*(5), 2383–2398. doi:10.1152/jn.00413.2011

Mostert, P., Kok, P., & Lange, F. P. de. (2015). Dissociating sensory from decision processes in human perceptual decision making. *Sci Rep*, *5*, 18253. doi:10.1038/srep18253

Myers, N. E., Rohenkohl, G., Wyart, V., Woolrich, M. W., Nobre, A. C., & Stokes, M. G. (2015). Testing sensory evidence against mnemonic templates. *Elife*, *4*. doi:10.7554/eLife.09000

Park, H., Lueckmann, J.-M., Kriegstein, K. von, Bitzer, S., & Kiebel, S. J. (2016). Spatiotemporal dynamics of random stimuli account for trial-to-trial variability in perceptual decision making. *Sci Rep*, *6*, 18832. doi:10.1038/srep18832

Pearson, J. M., Heilbronner, S. R., Barack, D. L., Hayden, B. Y., & Platt, M. L. (2011). Posterior cingulate cortex: adapting behavior to a changing world. *Trends in cognitive sciences*, *15*(4), 143–151. doi:10.1016/j.tics.2011.02.002

Philiastides, M. G., Heekeren, H. R., & Sajda, P. (2014). Human Scalp Potentials Reflect a Mixture of Decision-Related Signals during Perceptual Choices. *J Neurosci*, *34*(50), 16877–16889. doi:10.1523/JNEUROSCI.3012-14.2014

Philiastides, M. G., Ratcliff, R., & Sajda, P. (2006). Neural representation of task difficulty and decision making during perceptual categorization: a timing diagram. *The Journal of neuroscience : the official journal of the Society for Neuroscience*, *26*(35), 8965–8975. doi:10.1523/JNEUROSCI.1655-06.2006

Philiastides, M. G., & Sajda, P. (2006). Temporal characterization of the neural correlates of perceptual decision making in the human brain. *Cereb Cortex*, *16*(4), 509–518. doi:10.1093/cercor/bhi130

Selen, L. P. J., Shadlen, M. N., & Wolpert, D. M. (2012). Deliberation in the motor system: reflex gains track evolving evidence leading to a decision. *J Neurosci*, *32*(7), 2276–2286. doi:10.1523/JNEUROSCI.5273-11.2012

Smulders, F. T. Y., & Miller, J. O. (2012). The Lateralized Readiness Potential. In E. S. Kappenman & S. J. Luck (Eds.), *The Oxford Handbook of Event-Related Potential Components*. Oxford University Press. doi:10.1093/oxfordhb/9780195374148.013.0115

Taulu, S., Simola, J., & Kajola, M. (2005). Applications of the Signal Space Separation Method. *IEEE Transactions on Signal Processing*, *53*(9), 3359–3372. doi:10.1109/TSP.2005.853302

Thura, D., & Cisek, P. (2014). Deliberation and Commitment in the Premotor and Primary Motor Cortex during Dynamic Decision Making. *Neuron*, *81*(6), 1401–1416. doi:10.1016/j.neuron.2014.01.031

Thura, D., & Cisek, P. (2017). The Basal Ganglia Do Not Select Reach Targets but Control the Urgency of Commitment. *Neuron*, *95*(5), 1160–1170.e5. doi:10.1016/j.neuron.2017.07.039

Tosoni, A., Galati, G., Romani, G. L., & Corbetta, M. (2008). Sensory-motor mechanisms in human parietal cortex underlie arbitrary visual decisions. *Nature neuroscience*, *11*(12), 1446–1453. doi:10.1038/nn.2221

Wang, X.-J. (2008). Decision making in recurrent neuronal circuits. *Neuron*, *60*(2), 215–234. doi:10.1016/j.neuron.2008.09.034

Wyart, V., Gardelle, V. de, Scholl, J., & Summerfield, C. (2012). Rhythmic Fluctuations in Evidence Accumulation during Decision Making in the Human Brain. *Neuron*, *76*(4), 847–858. doi:10.1016/j.neuron.2012.09.015

Supplementary Information

Correlations with accumulated evidence

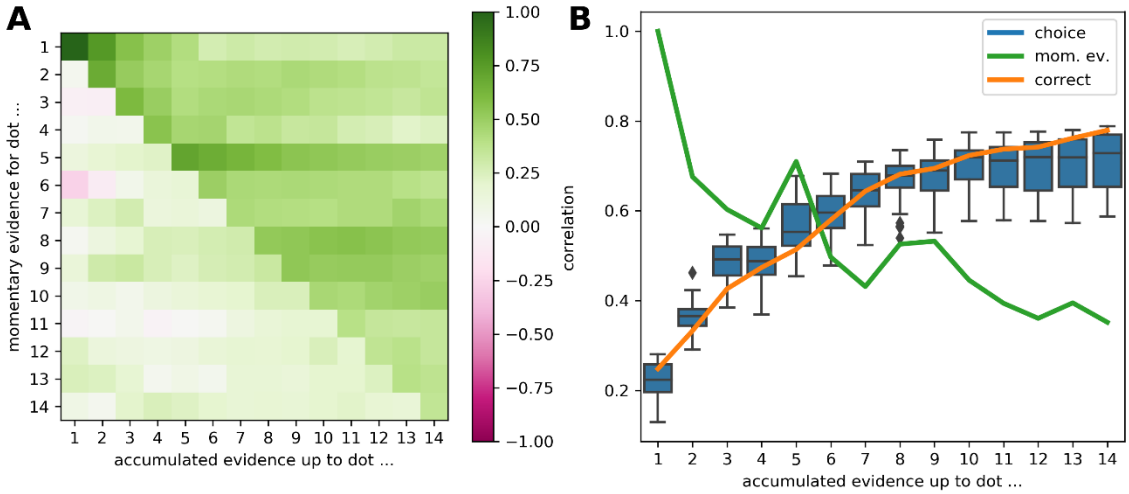

Supplementary Figure 1. The accumulated evidence is correlated across trials with the momentary evidence provided by dot positions, the correct choice in a trial and the choices of the participants. A: Correlation coefficients for all combinations of momentary and accumulated evidence for the shown onset times. For example, the correlation value at row 2, column 4 gives the correlation between the momentary evidence of the 2nd dot position within a trial and the accumulated evidence up to the 4th dot position, across trials. **B**: Comparison of correlations between accumulated evidence and three trial-wise measures: the correct choice in a trial (orange line), the momentary evidence at the same time point (green line, equal to diagonal in A), and the choices of the participants (blue boxes). The blue boxes show the distribution over participants per considered dot position.

Stereotyped temporal correlation profiles across evidence regressors

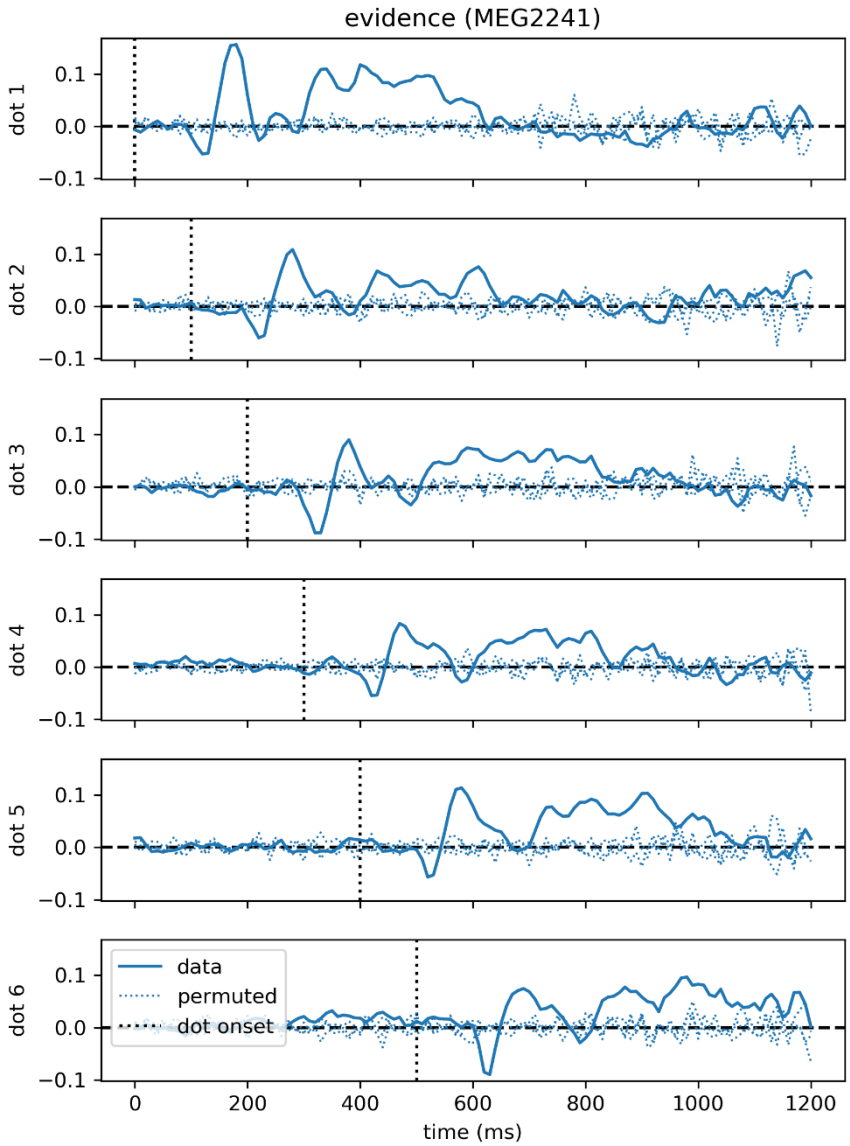

Supplementary Figure 2. Time course of correlations with decision evidence repeats for each dot shifted by dot onset times. In the standard regression analysis there was one regressor for each element in the sequence of dot positions (dots). This allowed us to see, when after first dot onset, correlations with the considered dot could be observed. The figure demonstrates exemplarily for the magnetometer channel with the strongest average correlations that the correlation time course exhibits roughly a stereotyped profile relative to the onset time of the dot on the second level. Dotted lines show the same quantity, but for data that we permuted over trials before the regression analysis.

All significant correlations with decision evidence

Supplementary Table 1. Overview over all significant correlations with decision evidence after FDR multiple comparison correction. Consecutive effects are aggregated into temporal clusters for which start and end times are noted. For each cluster we report the sum of log10p ($\log_{10}$(p-value) of the second-level t-test after multiple comparison correction) across the time points in the cluster. Clusters are sorted according to their start time.

label	region	start_t	end_t	log10p
L_V1	primary visual cortex	110	130	-11.677
R_VVC	ventral stream visual cortex	110	130	-7.444
R_V1	primary visual cortex	110	130	-10.711
R_V4	early visual cortex	110	140	-10.139

R_DVT	posterior cingulate cortex	110	130	-6.232
R_VMV2	ventral stream visual cortex	110	130	-7.680
L_LO3	MT+ complex and neighboring visual areas	110	130	-7.339
L_v23ab	posterior cingulate cortex	120	130	-4.163
L_VMV2	ventral stream visual cortex	120	130	-4.473
L_V4	early visual cortex	120	130	-6.491
L_TPOJ3	temporo-parieto-occipital junction	120	120	-2.406
R_VMV1	ventral stream visual cortex	120	130	-4.980
L_FST	MT+ complex and neighboring visual areas	120	130	-4.421
R_d23ab	posterior cingulate cortex	120	120	-2.347
L_MIP	superior parietal cortex	120	130	-5.393
R_31pv	posterior cingulate cortex	120	120	-2.152
R_FFC	ventral stream visual cortex	120	120	-2.078
R_v23ab	posterior cingulate cortex	120	130	-4.567
R_MT	MT+ complex and neighboring visual areas	120	120	-2.006
R_LO1	MT+ complex and neighboring visual areas	120	130	-4.443
R_MST	MT+ complex and neighboring visual areas	120	120	-2.078
L_MT	MT+ complex and neighboring visual areas	130	130	-2.121
L_V3	early visual cortex	130	130	-2.113
R_IP0	inferior parietal cortex	160	190	-9.066
R_TPOJ3	temporo-parieto-occipital junction	160	170	-4.436
R_PGp	inferior parietal cortex	170	170	-2.039
L_POS2	posterior cingulate cortex	170	190	-6.247
R_VIP	superior parietal cortex	170	190	-6.639
R_5mv	paracentral lobular and mid cingulate cortex	170	170	-2.074
R_7Am	superior parietal cortex	170	180	-4.330
L_V2	early visual cortex	180	180	-2.406
L_2	somatosensory and motor cortex	180	180	-2.007
L_POS1	posterior cingulate cortex	180	180	-2.139
R_DVT	posterior cingulate cortex	190	190	-2.139
R_V8	ventral stream visual cortex	200	200	-2.068
L_AIP	superior parietal cortex	290	290	-2.083
R_5mv	paracentral lobular and mid cingulate cortex	290	310	-6.404
R_31a	posterior cingulate cortex	300	300	-2.152
R_5m	paracentral lobular and mid cingulate cortex	300	300	-2.042
L_d23ab	posterior cingulate cortex	310	310	-2.105
R_31pd	posterior cingulate cortex	320	340	-7.789
L_p24pr	anterior cingulate and medial prefrontal cortex	320	320	-2.272
L_SCEF	paracentral lobular and mid cingulate cortex	320	320	-2.088
R_FEF	premotor cortex	320	320	-2.270
R_p24pr	anterior cingulate and medial prefrontal cortex	320	340	-6.715
R_7m	posterior cingulate cortex	320	340	-8.503
L_3a	somatosensory and motor cortex	320	330	-4.250
R_v23ab	posterior cingulate cortex	320	340	-7.525
L_31pd	posterior cingulate cortex	320	340	-6.768
R_24dv	paracentral lobular and mid cingulate cortex	320	320	-2.485
L_24dv	paracentral lobular and mid cingulate cortex	320	320	-2.282
R_1	somatosensory and motor cortex	330	330	-2.119
R_3b	somatosensory and motor cortex	330	330	-2.168

L_3b	somatosensory and motor cortex	330	340	-4.230
L_PCV	posterior cingulate cortex	330	340	-5.248
L_v23ab	posterior cingulate cortex	330	340	-4.302
R_PCV	posterior cingulate cortex	340	340	-2.139
L_31pv	posterior cingulate cortex	340	340	-2.270
R_FEF	premotor cortex	340	340	-2.282
L_d23ab	posterior cingulate cortex	340	340	-2.194
R_d23ab	posterior cingulate cortex	340	340	-2.282
R_31pv	posterior cingulate cortex	340	340	-2.282
L_4	somatosensory and motor cortex	380	420	-11.320
R_AIP	superior parietal cortex	390	400	-4.348
L_31pv	posterior cingulate cortex	400	410	-4.320
R_RSC	posterior cingulate cortex	400	400	-2.139
R_31pd	posterior cingulate cortex	410	410	-2.111
R_4	somatosensory and motor cortex	410	410	-2.007
R_7m	posterior cingulate cortex	410	410	-2.152
L_3a	somatosensory and motor cortex	410	410	-2.139
R_v23ab	posterior cingulate cortex	410	410	-2.020
R_3a	somatosensory and motor cortex	410	410	-2.074
R_d23ab	posterior cingulate cortex	430	430	-2.272
R_31pv	posterior cingulate cortex	430	440	-4.411
L_31pd	posterior cingulate cortex	430	430	-2.111
R_7m	posterior cingulate cortex	430	440	-4.250
R_31pd	posterior cingulate cortex	430	440	-4.383
R_V6	dorsal stream visual cortex	440	440	-2.031
R_RI	early auditory cortex	440	440	-2.168
R_DVT	posterior cingulate cortex	480	480	-2.111
L_31pd	posterior cingulate cortex	480	480	-2.058
L_3a	somatosensory and motor cortex	480	490	-4.258
L_4	somatosensory and motor cortex	480	500	-8.544
L_6d	premotor cortex	480	490	-4.485
L_v23ab	posterior cingulate cortex	480	490	-4.371
R_31pd	posterior cingulate cortex	480	480	-2.250
R_7m	posterior cingulate cortex	480	480	-2.290
R_AIP	superior parietal cortex	480	480	-2.270
L_7m	posterior cingulate cortex	480	480	-2.111
R_v23ab	posterior cingulate cortex	480	490	-4.678
R_3a	somatosensory and motor cortex	490	490	-2.406

Numerical values plotted in Figure 4

Supplementary Table 2. Average effect values plotted in **Figure 4** for each of the 34 brain areas with significant decision evidence correlations within 300 to 500 ms after dot onset. Values are sorted according to average mlog10p ($-\log_{10}$(p-value) of the second-level t-test) for that area.

label	region	mlog10p	tval	mean	std
L_4	somatosensory and motor cortex	3.940	4.357	0.020	0.028
R_7m	posterior cingulate cortex	3.699	-4.134	-0.022	0.032
R_v23ab	posterior cingulate cortex	3.693	-4.148	-0.025	0.036
R_31pd	posterior cingulate cortex	3.586	-4.052	-0.022	0.032

L_3a	somatosensory and motor cortex	3.476	-3.990	-0.020	0.029
L_v23ab	posterior cingulate cortex	3.399	3.919	0.024	0.036
L_31pd	posterior cingulate cortex	3.358	3.875	0.022	0.034
R_31pv	posterior cingulate cortex	3.269	-3.804	-0.019	0.029
L_3b	somatosensory and motor cortex	3.260	-3.815	-0.019	0.029
R_d23ab	posterior cingulate cortex	3.244	-3.783	-0.019	0.029
L_31pv	posterior cingulate cortex	3.229	3.779	0.018	0.028
R_AIP	superior parietal cortex	3.142	3.705	0.017	0.026
L_7m	posterior cingulate cortex	3.111	3.680	0.022	0.035
R_3a	somatosensory and motor cortex	3.103	3.678	0.015	0.023
R_V6	dorsal stream visual cortex	3.096	-3.649	-0.021	0.033
L_d23ab	posterior cingulate cortex	2.992	3.577	0.017	0.029
R_4	somatosensory and motor cortex	2.896	-3.511	-0.014	0.024
L_PCV	posterior cingulate cortex	2.717	3.281	0.016	0.029
L_6d	premotor cortex	2.653	-3.262	-0.014	0.024
R_3b	somatosensory and motor cortex	2.563	3.211	0.014	0.025
R_p24pr	anterior cingulate and medial prefrontal cortex	2.453	3.090	0.014	0.027
R_PCV	posterior cingulate cortex	2.451	-3.043	-0.016	0.031
R_FEF	premotor cortex	2.403	3.042	0.012	0.024
R_24dv	paracentral lobular and mid cingulate cortex	2.353	2.999	0.013	0.026
R_31a	posterior cingulate cortex	2.324	-2.962	-0.014	0.027
R_RSC	posterior cingulate cortex	2.096	-2.791	-0.011	0.023
R_RI	early auditory cortex	2.041	2.718	0.012	0.026
R_DVT	posterior cingulate cortex	2.002	-2.631	-0.016	0.037
R_1	somatosensory and motor cortex	1.882	-2.542	-0.009	0.020
L_SCEF	paracentral lobular and mid cingulate cortex	1.746	-2.383	-0.010	0.026
L_24dv	paracentral lobular and mid cingulate cortex	1.643	-2.237	-0.010	0.027
L_p24pr	anterior cingulate and medial prefrontal cortex	1.613	-2.217	-0.010	0.027
R_5mv	paracentral lobular and mid cingulate cortex	1.610	-2.256	-0.011	0.028
R_5m	paracentral lobular and mid cingulate cortex	1.585	-2.186	-0.009	0.023

Time-course of response-aligned grand averages

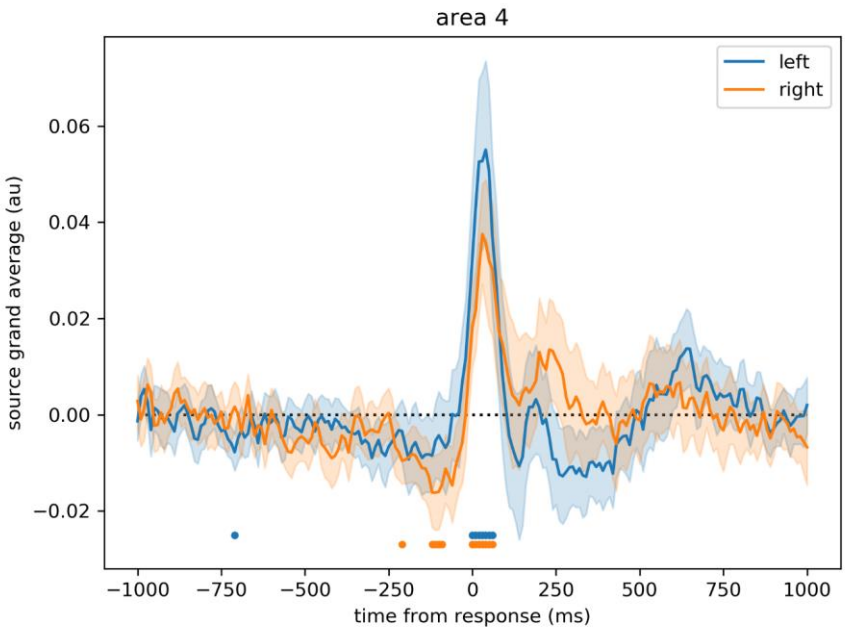

Supplementary Figure 3. Grand average source activations in left (blue) and right (orange) primary motor cortex (area 4). Shaded regions are +-2 standard errors of the mean of the second-level analysis across participants. Dots under the time courses indicate time points at which the grand average differs significantly from 0 after FDR-correction with α = 0.01. The peak across both hemispheres is reached 30 ms after the response.

Time courses of average magnitude of effects in source space

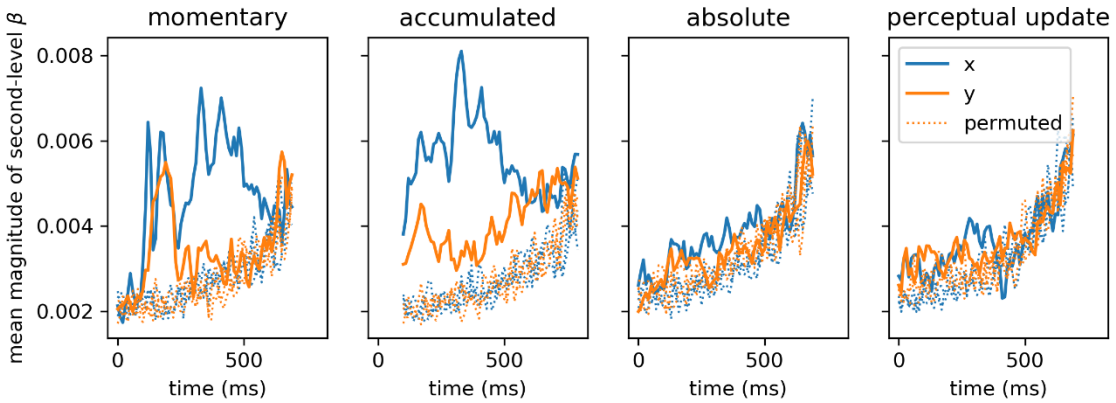

Supplementary Figure 4. Time courses from the expanded regression analysis in dot onset aligned time in source space. Values are mean (across brain areas) magnitude of second-level regression coefficients (β). Shown are effects for all used regressors (excluding the intercept). All regressors were derived from the dot positions. Regressors derived from x-coordinates (evidence) are shown in blue while y-coordinate regressors are shown in orange. For reference we also plotted regression coefficients obtained from permuted data as dotted lines. We included 4 different measures in our analysis: 'momentary' (evidence) are the original x- and y-coordinates (cf. **Figure 3**), 'accumulated' corresponds to summed coordinates, but only up to the previous dot (see Methods), 'absolute' are the absolute coordinates measuring only the displacement of the dot from 0 in both directions and 'perceptual update' is the absolute difference between the latest and the previous dot positions (cf. Wyart et al., 2012). Only the regressors respecting the sign of the coordinates (momentary and accumulated) exhibit strong effects. Note that we shifted the effects for the accumulated regressors 100 ms to the right to account for them being defined for the previous dot position instead of the current ones as for the other regressors. Also, the effects measured with the accumulated regressors, although accumulated and momentary regressors were uncorrelated, are a mixture of effects attributable to raw x-, y-coordinates and their cumulative sum, because accumulated regressors of dot *d*-1, although being uncorrelated to momentary regressors of dot *d,* are correlated with momentary regressors of dot *d*-1 and earlier.